Journal of Applied Research in Optics and Laser Technology,Volume 1, Number 5, Summer 2026

MoS_2-Enhanced Toothed Plasmonic Waveguide Sensor for High-Sensitivity Biosensing

Fariba Lotfi [*,1], Reza Kheradmand[1]

[1] *Department of Physics, University of Tabriz, Tabriz, Iran*

Received: 2026-07-03 Final revised: 2026-08-20 Accepted: 2026-09-15

Abstract

We design a toothed plasmonic waveguide sensor with a monolayer MoS_2 located at the metal–dielectric interface and compare its sensing performance with graphene under the same conditions. We optimize the rectangular-tooth dimensions to enhance the interaction between the confined plasmonic field and the surrounding sensing medium. The optimized structure achieves a maximum refractive-index sensitivity of 896 nm/RIU for a tooth size of 80 nm × 50 nm over an RI range of 1.33–1.40. We further evaluate the sensing performance using the refractive indices of healthy tissue, basal cell, and melanoma samples. The transmission spectra show distinct resonance shifts for the different biological samples, demonstrating the sensor's ability to distinguish small refractive-index variations. The basal cell sample achieves a maximum sensitivity of 880 nm/RIU. The comparative analysis shows that MoS_2 provides higher sensitivity than graphene in the proposed configuration and enhances the optical response of the plasmonic waveguide. These results indicate that the proposed sensor offers a compact and highly sensitive platform for refractive-index-based biomedical detection.

Keywords: Plasmonic sensor; MoS_2; Basal cell; Refractive-index sensor; Sensitivity

*Corresponding Author: f.lotfi@tabrizu.ac.ir

1. Introduction

Plasmonic sensors have attracted considerable attention in nanophotonics because they can confine electromagnetic fields at metal–dielectric interfaces and provide high sensitivity to changes in the surrounding refractive index. Surface plasmon polaritons (SPPs) are electromagnetic waves associated with collective electron oscillations at a metal–dielectric boundary. Their strong field localization near the interface enables plasmonic structures to detect small changes in the optical properties of the surrounding medium, which has led to their extensive use in chemical and biological sensing [1, 2]. In addition, plasmonic waveguides can confine optical modes beyond the conventional diffraction limit, providing a compact platform for integrated sensing and nanophotonic devices [2, 3].

The sensing performance of a plasmonic structure strongly depends on the distribution of the electromagnetic field and its interaction with the surrounding medium. In particular, the metal–dielectric interface plays a critical role because the SPP field reaches its maximum intensity in the vicinity of this boundary. However, metallic materials also introduce optical losses that can broaden resonances and limit the performance of plasmonic devices. Researchers have therefore explored different waveguide geometries and hybrid material configurations to improve field confinement and sensing characteristics [3, 4].

Two-dimensional (2D) materials have emerged as promising materials for plasmonic and optical sensing because of their atomically thin structures and distinctive optical and electronic properties. Graphene represents one of the most extensively studied 2D materials in plasmonics. Its high carrier mobility, broadband optical response, and tunable electrical properties have enabled its integration with plasmonic structures for sensing and other nanophotonic functions[5, 6]. However, transition metal dichalcogenides (TMDs) provide an alternative class of 2D materials with different optical characteristics that can be advantageous for visible and near-infrared photonic structures.

Among TMDs, molybdenum disulfide (MoS_2) has received particular attention because monolayer MoS_2 exhibits a direct bandgap and pronounced optical resonances in the visible spectral region [7, 8]. Its optical response differs substantially from that of graphene, providing an additional degree of freedom for controlling the electromagnetic response of hybrid plasmonic structures. Experimental and theoretical studies have also established the importance of accurately describing the wavelength-dependent complex optical constants of MoS_2 when analyzing its interaction with electromagnetic fields [8]. Recent reviews further indicate that MoS_2 and other 2D materials can modify the optical response of metal interfaces and improve the performance of surface plasmon resonance sensors [9].

The location of a 2D material within a plasmonic structure is also important. Placing the material close to the region of maximum plasmonic-field intensity increases its electromagnetic interaction with the guided mode. Therefore, locating a MoS_2 monolayer directly at the metal–dielectric interface can provide an effective approach for modifying the modal characteristics of a plasmonic waveguide. In such a configuration, the optical properties of MoS_2 directly influence the local dielectric environment experienced by the plasmonic mode. This effect can alter the resonance condition and increase the spectral response to changes in the refractive index of the sensing medium [9].

In parallel with material engineering, geometric engineering provides another effective method for controlling plasmonic modes. Dielectric-loaded plasmonic waveguides can

support strongly confined modes, while variations in the dimensions and arrangement of dielectric features can modify mode confinement, effective index, and propagation characteristics [4, 10]. In particular, nanoscale protrusions or teeth can locally perturb the guided mode and increase the interaction between the electromagnetic field and the sensing region. Combining such geometrical features with an atomically thin material at the metal–dielectric interface can therefore provide a suitable platform for improving refractive-index sensitivity.

In this work, we develop a toothed plasmonic waveguide sensor in which a monolayer MoS_2 is located directly at the metal–dielectric interface. We analyze the effect of the rectangular-tooth dimensions on the sensing response and compare the MoS_2 configuration with an equivalent graphene-based structure under identical geometrical conditions. We consider sensing media with refractive indices from 1.33 to 1.40 and identify the geometry that provides the highest wavelength sensitivity. We then evaluate the optimized MoS_2 structure for basal cell and melanoma samples. The proposed configuration achieves a maximum refractive-index sensitivity of 896 nm/RIU, while a sensitivity of 880 nm/RIU is obtained for the basal cell sample. These results show the potential of interface-located MoS_2 for improving the refractive-index response of toothed plasmonic waveguide sensors.

2 .Theory and Methodology

The sensing mechanism of the proposed structure relies on the sensitivity of the plasmonic mode to changes in the refractive index of the surrounding medium. Surface plasmon polaritons (SPPs) propagate along a metal–dielectric interface and exhibit strong electromagnetic-field confinement near the interface. Consequently, a change in the dielectric environment modifies the propagation characteristics of the plasmonic mode and shifts its spectral response [11, 12].

For a planar interface between a metal with permittivity ε_m and a dielectric with permittivity ε_d, the SPP propagation constant can be expressed as

$$\beta_{\mathrm{SPP}} = k_0\sqrt{\frac{\varepsilon_m\varepsilon_d}{\varepsilon_m+\varepsilon_d}}, \tag{1}$$

where $k_0 = 2\pi/\lambda$ is the free-space wavenumber, and ε_m and ε_d denote the complex permittivities of the metal and dielectric, respectively [11, 12]. Equation (1) indicates that variations in the dielectric environment directly affect the propagation constant of the plasmonic mode. Therefore, changes in the refractive index of the sensing region can be detected through the resulting spectral shift.

We describe the electromagnetic response of the proposed structure using the frequency-domain form of Maxwell's equations. For a linear, isotropic, and source-free medium, the electric-field distribution is obtained from

$$\nabla \times (\mu_r^{-1}\nabla \times E) - k_0^2\varepsilon_r E = 0, \tag{2}$$

where E represents the electric-field vector, μ_r is the relative permeability, and ε_r is the complex relative permittivity of the medium. We solve this equation using the finite element method (FEM) to determine the electromagnetic response of the proposed plasmonic waveguide.

The optical properties of the constituent materials are described using their complex refractive indices. The corresponding complex relative permittivity is given by

$$\varepsilon_r = (n + ik)^2, \tag{3}$$

where n is the real part of the refractive index and k is the extinction coefficient. For the

MoS_2 layer, we use wavelength-dependent optical constants to account for its dispersive response. Experimental spectroscopic studies have reported significant wavelength dependence in the refractive index and extinction coefficient of monolayer MoS_2, confirming the importance of using appropriate optical data in the modeling of MoS_2-based photonic structures [13,14].

We locate the monolayer MoS_2 directly at the metal–dielectric interface, where the plasmonic field is strongly confined. The presence of this atomically thin layer modifies the local optical environment of the plasmonic mode. Since monolayer MoS_2 has distinct optical properties and a thickness of approximately 0.6–0.7 nm, it can be represented as an ultrathin dispersive layer in the numerical model [13, 14].

We evaluate the sensing response by monitoring the resonance wavelength as the refractive index of the sensing region changes. The wavelength sensitivity is calculated according to

$$S_\lambda = \frac{\Delta\lambda_{\mathrm{res}}}{\Delta n}, \quad (4)$$

where $\Delta\lambda_{\mathrm{res}}$ represents the resonance-wavelength shift and Δn is the corresponding change in refractive index. The sensitivity is expressed in nm/RIU. This parameter provides a direct measure of the spectral response of the plasmonic sensor to variations in the refractive index.

We apply the same theoretical approach to the graphene-based configuration to provide a direct comparison with the proposed MoS_2 structure. We maintain the same geometrical parameters and sensing conditions and replace the MoS_2 layer with graphene. This procedure allows us to evaluate the effect of the 2D material on the sensing response without introducing changes associated with different geometrical configurations.

We first vary the dimensions of the rectangular teeth to determine the geometry that provides the highest refractive-index sensitivity. We then use the optimized geometry for a direct comparison between the MoS_2- and graphene-based configurations. Finally, we evaluate the optimized MoS_2 structure using the refractive-index values associated with basal cell and melanoma samples. This methodology enables us to separately assess the effects of the tooth geometry and the selected 2D material on the sensing performance.

2.1 Theoretical Background

We describe the optical response of the metallic layer using the Drude model, which accounts for the contribution of free electrons to the frequency-dependent dielectric function of the metal. The complex relative permittivity of the metal is expressed as

$$\varepsilon_{\mathrm{m}}(\omega) = \varepsilon\infty - {\omega_{\mathrm{p}}}^2/(\omega^2 + i\gamma\omega), \quad (5)$$

where $\varepsilon\infty$ is the contribution of bound electrons, ω_p is the plasma frequency, γ is the electron collision frequency, and ω is the angular frequency of the incident electromagnetic wave. The plasma frequency is defined as

$$\omega_{\mathrm{p}} = \sqrt{(n_{\mathrm{e}}e^2/\varepsilon_0 * m)}, \quad (6)$$

where n_e is the free-electron density, e is the elementary charge, ε_0 is the vacuum permittivity, and m* is the effective electron mass. The complex refractive index of the metal is related to its dielectric function through

$$\tilde{n}_{\mathrm{m}} = n_{\mathrm{m}} + ik_{\mathrm{m}} = \sqrt{\varepsilon_{\mathrm{m}}}, \quad (7)$$

where n_m and k_m represent the real and imaginary parts of the refractive index, respectively. The Drude model provides the frequency-dependent dielectric response

required to describe the optical behavior of the metallic layer and the formation of plasmonic modes at the metal–dielectric interface [15, 16].

We describe monolayer MoS_2 using its complex wavelength-dependent refractive index, which is expressed as

$$\tilde{n}MoS_2(\lambda) = nMoS_2(\lambda) + ikMoS_2(\lambda), \quad (8)$$

where n_{MoS_2} and k_{MoS_2} represent the real and imaginary parts of the refractive index, respectively. The corresponding complex relative permittivity is obtained from

$$\varepsilon MoS_2(\lambda) = [nMoS_2(\lambda) + ikMoS_2(\lambda)]^2. \quad (9)$$

We use wavelength-dependent optical constants for monolayer MoS_2 because its optical response differs from that of bulk MoS_2 and exhibits significant spectral dispersion [13, 14]. In the proposed structure, the MoS_2 layer is located directly at the metal–dielectric interface and is modeled as an ultrathin layer with a thickness of approximately 0.65 nm. The position of this layer is particularly important because the plasmonic electromagnetic field is strongly confined near the metal–dielectric interface. Therefore, the presence of MoS_2 modifies the local optical environment of the plasmonic mode through its complex wavelength-dependent permittivity. We describe the effect of MoS_2 solely through its optical constants and do not consider plasmon–exciton coupling in the present theoretical model.

We describe graphene using its frequency-dependent surface conductivity based on the Kubo formalism. The total graphene conductivity is expressed as

$$\sigma g(\omega, \mu c, \Gamma, T) = \sigma intra + \sigma inter, \quad (10)$$

where μ_c is the chemical potential, T is the temperature, and Γ is the carrier scattering rate. The intraband contribution is given by

$$\sigma_{intra}(\omega) = \frac{2ik_BTe^2}{\pi\hbar^2(\omega+{}^{i}/_{\tau})} ln\left[2cosh\left(\frac{E_f}{2k_BT}\right)\right], \quad (11)$$

where kB is the Boltzmann constant and $\hbar$ is the reduced Planck constant. The interband contribution is expressed as

$$\sigma_{inter}(\omega) = \frac{e^2}{4\hbar}\left[\frac{1}{2} + \frac{1}{\pi} arctan\frac{\hbar\omega-2E_f}{2k_BT} - \frac{i}{2\pi} ln\frac{(\hbar\omega+2E_f)^2}{(\hbar\omega-2E_f)^2+(2k_BT)^2}\right]. \quad (12)$$

The Kubo formalism describes the frequency-dependent surface conductivity of graphene as a function of chemical potential, temperature, and carrier scattering. We use this conductivity to represent graphene as a two-dimensional conducting layer in the comparative configuration. This approach is widely used for modeling the electromagnetic response of graphene in plasmonic structures and provides a consistent basis for comparing graphene with other two-dimensional materials [17-19].

The optical models described above provide the material parameters required for the numerical analysis of the proposed plasmonic waveguide. We use the Drude model to describe the dispersive response of the metallic layer, wavelength-dependent complex optical constants to represent monolayer MoS_2, and the Kubo formalism to describe graphene. These material models allow the optical response of the MoS_2- and graphene-based configurations to be evaluated under the same structural conditions.

2.2 Numerical Model

Figure 1 shows the schematic configuration of the proposed plasmonic waveguide sensor, including the metal, dielectric, rectangular-tooth structure, sensing region, and monolayer MoS_2 located at the metal–dielectric interface. The proposed structure is

designed to confine the electromagnetic field near the metal–dielectric interface, where the presence of MoS_2 can affect the optical response of the plasmonic mode.
The geometric parameters of the structure are as follows:

L_1 = 600 nm, L_2 = 70nm, L_3 = 50 nm, L_4 = 170 nm w_1 = 400 nm and w_2 = 50 nm.

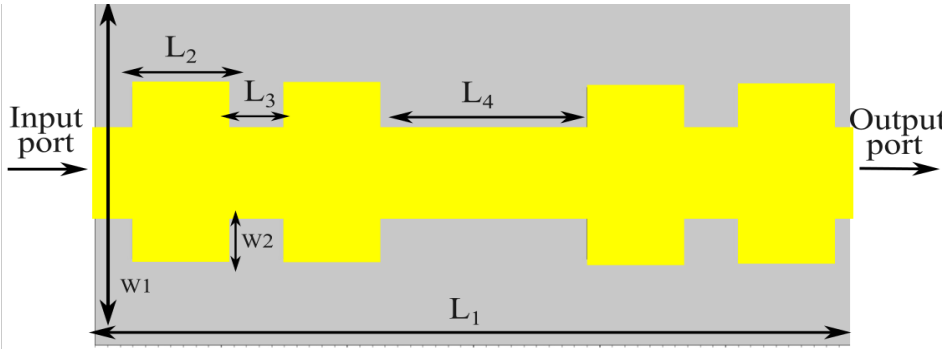


Fig. 1. Schematic of the designed plasmonic sensor made of MDM waveguides including MoS_2. The gray and yellow area are metal and air (or sample domain), respectively. The geometrical parameters of sensor structure are w_1=400nm, L_1=600nm, w_2=50nm, L_2=70nm, L_3=50nm and L_4=170nm.

We perform the numerical analysis using COMSOL Multiphysics based on the finite element method (FEM). A monolayer MoS_2 with a thickness of approximately 0.65 nm is located directly at the metal–dielectric interface. We describe the dispersive response of the metallic region using the Drude model and use wavelength-dependent complex optical constants for MoS_2. For comparison, we replace MoS_2 with graphene and describe its optical response using the Kubo conductivity model. The sensing region is filled with materials having refractive indices ranging from 1.33 to 1.40.

We excite the structure using a TM-polarized incident electromagnetic wave with an electric-field amplitude of 50 V/m. We perform the optical analysis in the wavelength domain and calculate the electromagnetic response of the structure over the selected wavelength range. We apply appropriate electromagnetic boundary conditions to the computational domain. A triangular mesh is used throughout the computational domain, with finer elements near the metal–dielectric interface, rectangular-tooth regions, and the ultrathin MoS_2 layer, where stronger field variations are expected. We perform mesh refinement to ensure that further reduction of the element size produces negligible changes in the calculated resonance positions.

We obtain the transmission spectrum from the calculated electromagnetic response and determine the resonance wavelength for each refractive index. We first optimize the dimensions of the rectangular tooth to obtain the highest sensing performance. We then compare the optimized MoS_2-based structure with the corresponding graphene-based configuration under identical geometrical and sensing conditions. Finally, we use the optimized MoS_2 structure to evaluate its response to the refractive indices associated with basal cell and melanoma samples. The obtained resonance shifts are used to calculate the refractive-index sensitivity and evaluate the sensing performance of the proposed structure.

3 . Results and Discussion

In this section, we analyze the sensing performance of the proposed MoS_2-assisted MDM waveguide. We first examine the transmission response and electromagnetic field distribution for different sample refractive indices ranging from 1.33 to 1.40. We then compare the proposed structure with a graphene-based configuration under the same conditions to evaluate the effect of the 2D material on sensitivity. The geometric parameters of the rectangular-tooth structure are subsequently optimized to achieve the highest sensitivity. Finally, the optimized sensor is evaluated using the refractive indices of basal cell and melanoma samples to assess its performance for biological detection.
Figure 2 shows the transmission spectra of the sensor without MoS_2 for refractive indices of 1.33–1.40. The resonance peak shifts with increasing refractive index. As shown in Figure 3, the sensitivity is determined from the slope of the linear fit to the resonance wavelength shift data, yielding 699 nm/RIU. After adding MoS_2 at the metal–dielectric interfaces, larger spectral shifts are observed, leading to higher sensitivity.

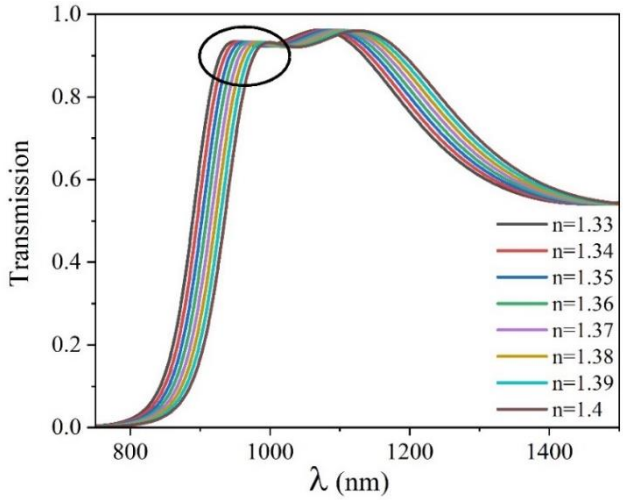


Fig. 2. Transmission spectra of the sensor structure without MoS_2 for the injecting of samples with refractive indices of 1.33 and 1.4 into the core of MDM waveguide.

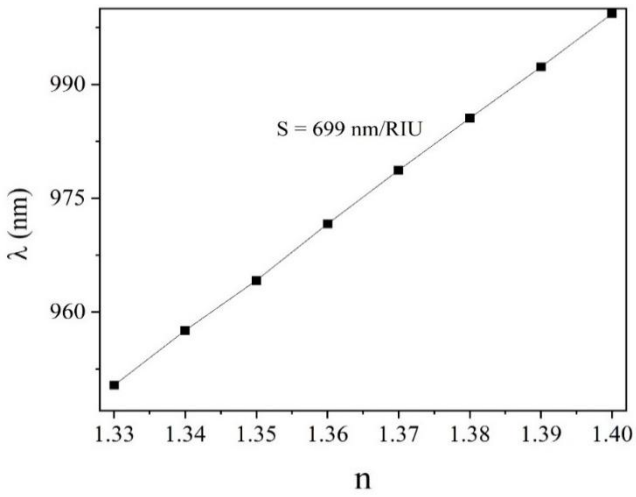


Fig. 3. Wavelength shift as a function of refractive index (ranging from 1.33 to 1.4) for the peak observed in the transmission spectra of Fig.2.

To verify mesh independence, four mesh levels, namely fine, finer, extra fine, and extremely fine, were tested for the sensor without MoS_2 at a sample refractive index of 1.33. As shown in Fig. 4, the transmission spectra obtained with the four mesh levels almost completely overlap around the resonance peak, with no noticeable shift in its position as the mesh is refined. This confirms that further mesh refinement does not produce a meaningful change in the calculated resonance wavelength. Therefore, the selected mesh provides sufficient numerical accuracy for the subsequent simulations.

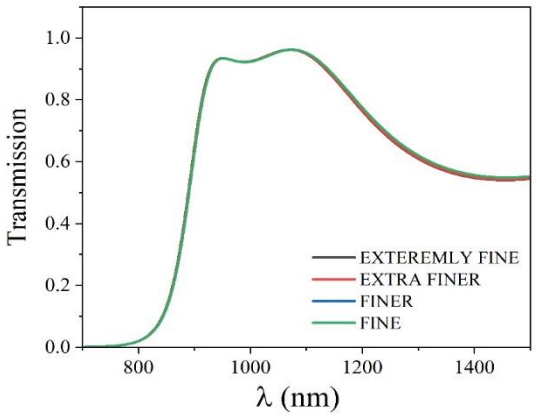


Fig. 4. Transmission spectra of the MDM waveguide sensor without MoS_2 for different mesh levels at a sample refractive index of 1.33.

Next, we employ a monolayer MoS_2 at the metal–dielectric interfaces, and the transmission spectra are obtained for sample refractive indices ranging from 1.33 to 1.40, as shown in Figure 5. The resonance peaks shift with increasing refractive index, and the sensitivity is determined from the slope of the linear fit to the peak-shift data in Figure 6. A sensitivity of 886 nm/RIU is obtained, compared with 699 nm/RIU for the structure without MoS_2. This improvement is attributed to the stronger electromagnetic field confinement near the metal–dielectric interfaces, which enhances the interaction between the plasmonic field and the sample.

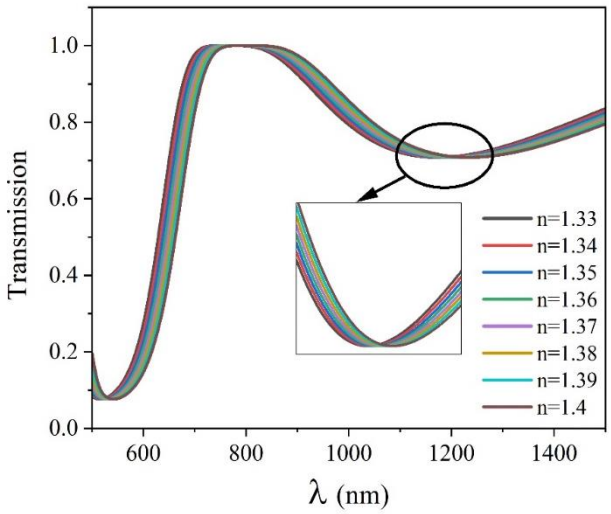


Fig. 5. Transmission spectra of the sensor structure with MoS_2 for the injecting of samples with refractive indices of 1.33 and 1.4 into the core of MDM waveguide.

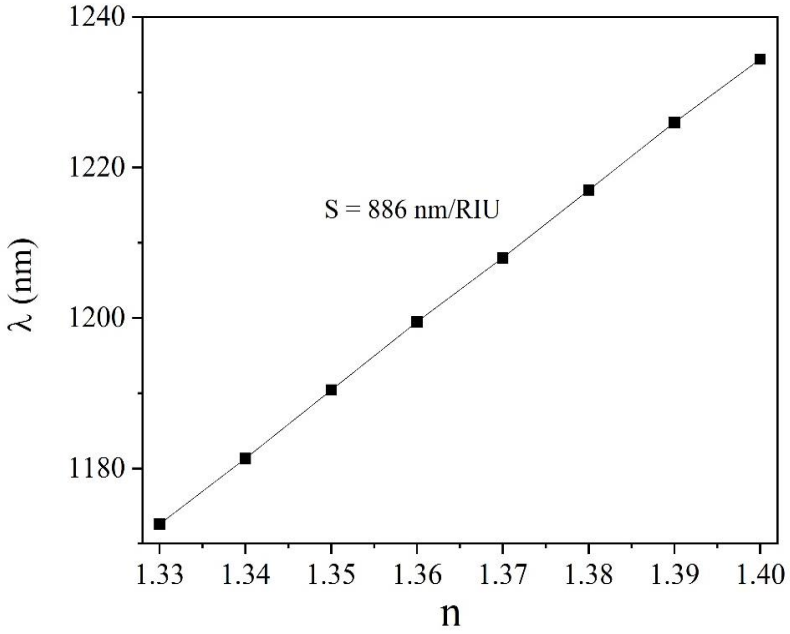


Fig. 6. Wavelength shift as a function of refractive index (ranging from 1.33 to 1.4) for the peak observed in the transmission spectra of Fig.4 for the sensor based MoS_2.

To evaluate the effect of the 2D material on the sensing performance, graphene is considered at the metal–dielectric interfaces using the same rectangular-tooth geometry and refractive-index range of 1.33–1.40. The transmission spectra of the graphene- and MoS_2-based configurations are compared under identical conditions, as shown in Figure 7. The graphene configuration exhibits smaller spectral shifts than the MoS_2-based structure, resulting in lower sensitivity. This comparison demonstrates the effect of the selected 2D material on the sensing response of the proposed MDM waveguide.

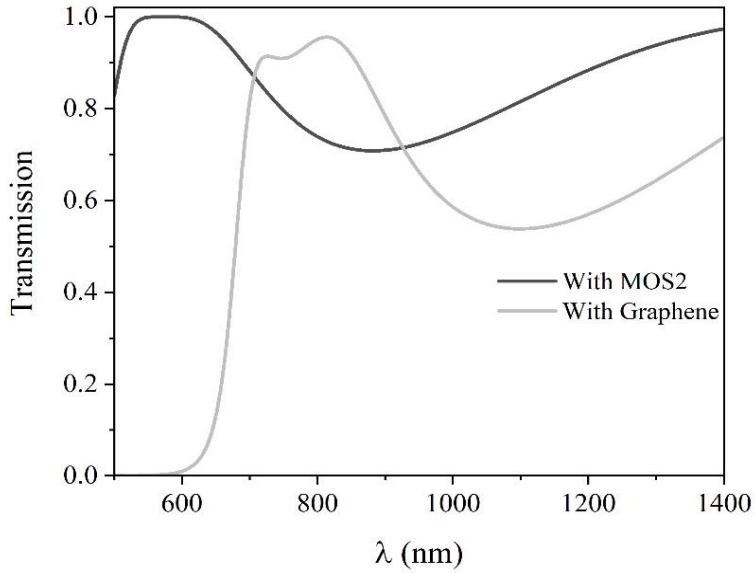


Fig. 7. Transmission spectra of the MDM waveguide sensor with and without a monolayer of MoS_2.

Figure 8 presents the transmission spectra of the graphene-assisted sensor for refractive indices ranging from 1.33 to 1.40. The sensitivity is determined from the slope of the linear fit to the resonance peak shifts, as shown in Figure 9, yielding 798 nm/RIU. This value is lower than the 886 nm/RIU obtained for the MoS_2-based configuration. The higher sensitivity of MoS_2 is attributed to its stronger effect on the electromagnetic field distribution at the metal–dielectric interface, resulting in larger resonance shifts for the same refractive-index variation.

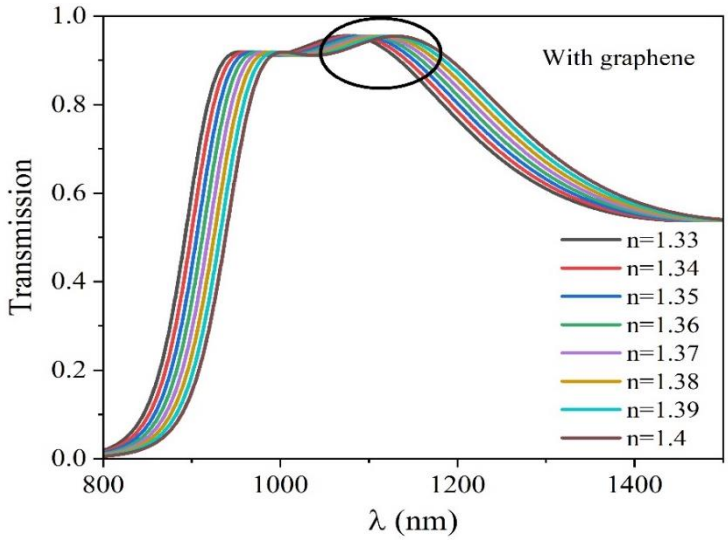


Fig. 8. Transmission spectra of the graphene-based sensor for samples with refractive indices of 1.33 and 1.40 injected into the core of the MDM waveguide, with graphene replacing MoS_2 at the metal–dielectric interfaces.

We evaluate the effect of the rectangular tooth length on the sensing performance of the MoS_2-assisted MDM waveguide. The tooth length is varied from 60 to 80 nm while keeping the other parameters unchanged, and the transmission peak shifts are analyzed for refractive indices of 1.33–1.40 in Figs. (10,12). The sensitivities obtained from the slopes of the linear fits are 875, 886, and 896 nm/RIU for tooth lengths of 60, 70, and 80 nm from Figs. (11,13), respectively. The highest sensitivity is therefore achieved at a tooth length of 80 nm, indicating that the tooth geometry significantly affects the sensing response.

We evaluate the effect of the rectangular tooth width on the sensing performance by varying the width from 40 to 60 nm while keeping the tooth length at 70 nm and the refractive-index range at 1.33–1.40. The sensitivities obtained from the linear fits of the resonance peak shifts, as shown in Figs. (14,16) are 856 and 854 nm/RIU for widths of 40 and 60 nm from Figs. (15,17), respectively. Both values are slightly lower than the sensitivity obtained with the original 50 nm width, indicating that the tooth width affects the field confinement and sensing response. Considering the combined optimization of tooth length and width, the highest sensitivity of 896 nm/RIU is achieved for a tooth dimension of 80 nm × 50 nm. Therefore, this geometry is selected as the optimized configuration for the subsequent analysis.

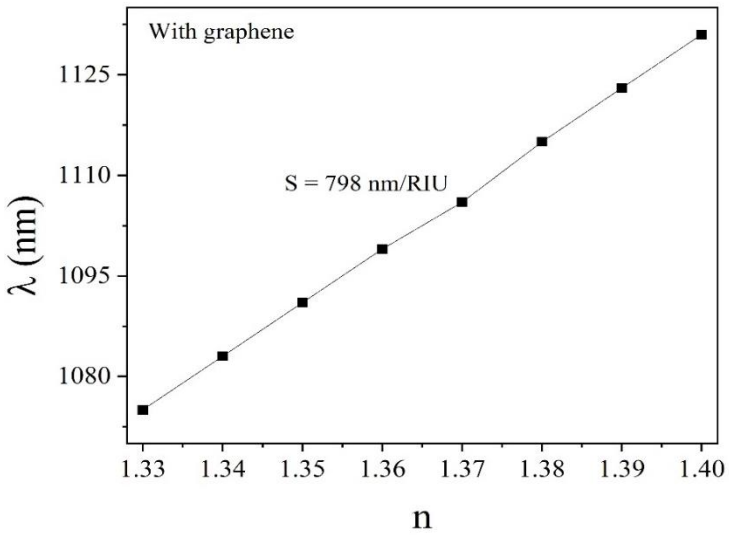


Fig. 9. Wavelength shift as a function of refractive index (ranging from 1.33 to 1.4) for the peak observed in the transmission spectra of Fig.7 for the sensor-based graphene.

We evaluate the optimized MoS_2-assisted MDM waveguide for distinguishing between basal cell and melanoma samples using their reported refractive indices. The corresponding refractive indices are applied to the sensing region, and the transmission spectra are calculated under identical simulation conditions. The two samples produce distinct resonance positions due to their different refractive indices, demonstrating the sensitivity of the optimized structure to small changes in the biological sample. The refractive indices used for basal cell and melanoma are summarized in Table 1 [20, 21]. A maximum sensitivity of 880 nm/RIU is obtained for the basal cell sample, confirming the suitability of the optimized MoS_2-based sensor for refractive-index-based differentiation of skin cancer samples.

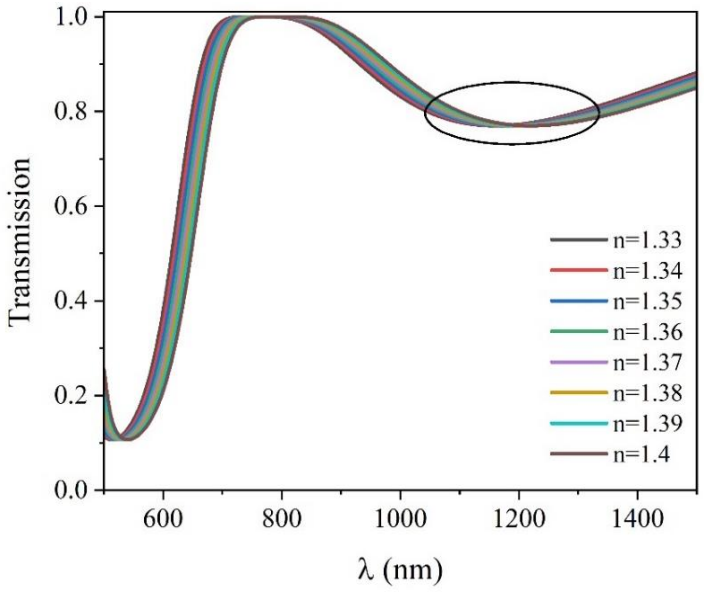


Fig. 10. Transmission spectra of the sensor structure with MoS_2 for the injecting of samples with refractive indices of 1.33 and 1.4 into the core of MDM waveguide for L_2=60 nm.

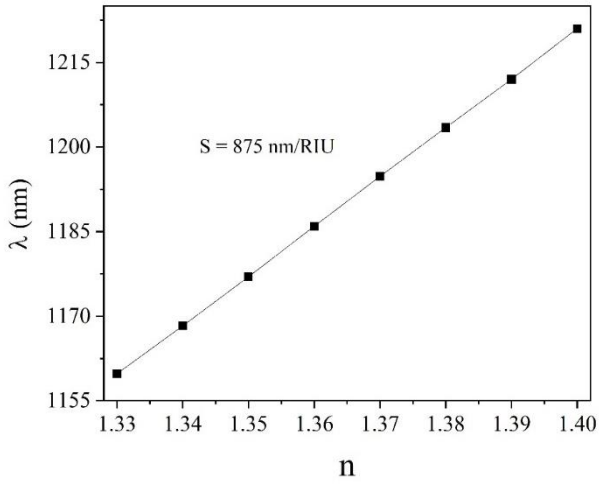


Fig. 11. Wavelength shift as a function of refractive index (ranging from 1.33 to 1.4) for the peak observed in the transmission spectra of Fig.9 for the sensor based MoS_2 with L_2=60 nm.

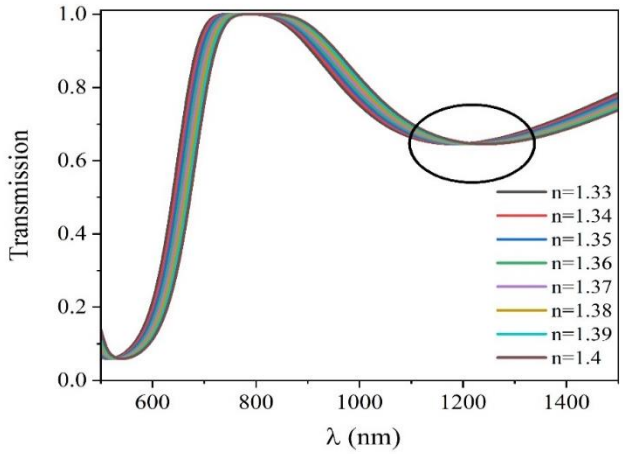


Fig. 12 . Transmission spectra of the sensor structure with MoS_2 for the injecting of samples with refractive indices of 1.33 and 1.4 into the core of MDM waveguide for L_2=80 nm.

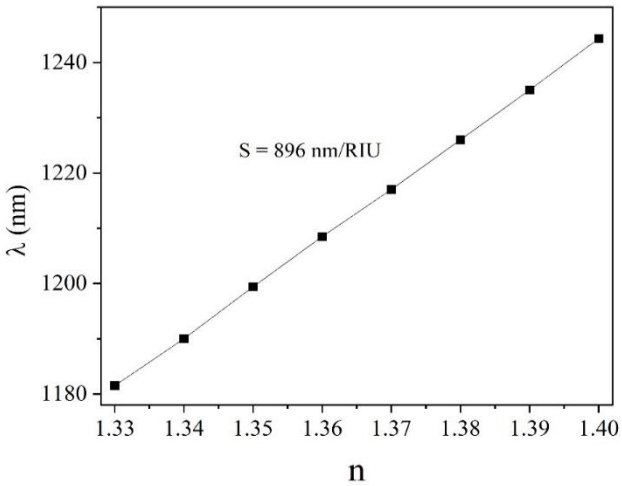


Fig. 13. Wavelength shift as a function of refractive index (ranging from 1.33 to 1.4) for the peak observed in the transmission spectra of Fig.11 for the sensor based MoS_2 with L_2=80 nm.

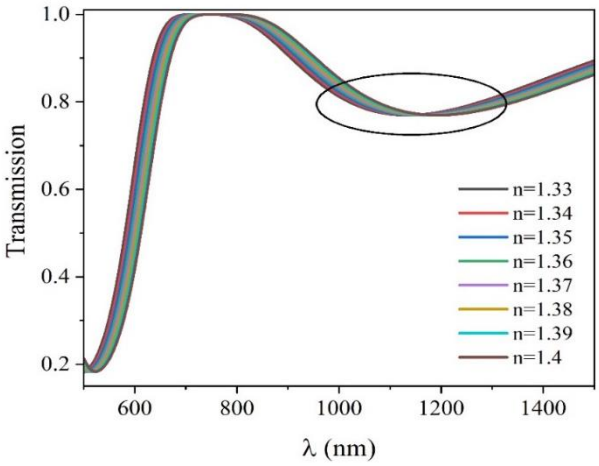


Fig. 14. Transmission spectra of the sensor structure with MoS_2 for the injecting of samples with refractive indices of 1.33 and 1.4 into the core of MDM waveguide for w_2=40 nm.

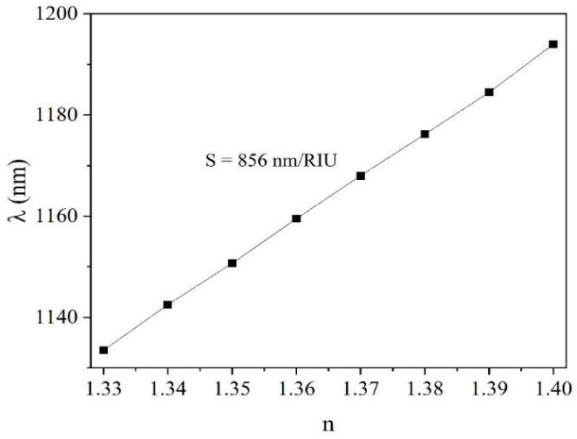


Figure 15. Wavelength shift as a function of refractive index (ranging from 1.33 to 1.4) for the peak observed in the transmission spectra of Fig.13 for the sensor based MoS_2 with w_2=40 nm.

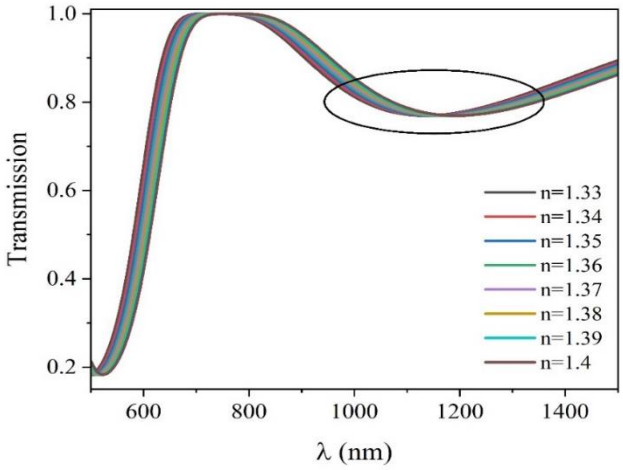


Fig. 16. Transmission spectra of the sensor structure with MoS_2 for the injecting of samples with refractive indices of 1.33 and 1.4 into the core of MDM waveguide for w_2=60 nm.

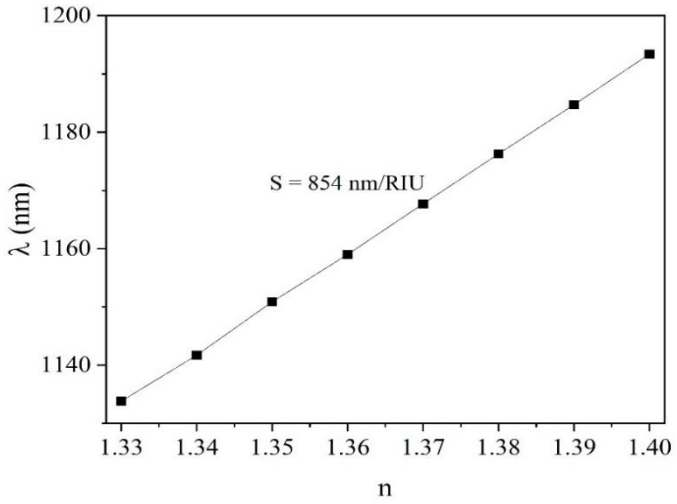


Fig. 17. Wavelength shift as a function of refractive index (ranging from 1.33 to 1.4) for the peak observed in the transmission spectra of Fig.15 for the sensor based MoS_2 with w_2=60 nm.

Table 1. Refractive index values of the normal and cancerous skin samples

Sample Type	Refractive Index
Basal normal cell	1.36
Basal cancer cell	1.38
Melanoma normal cell	1.38
Melanoma cancer cell	1.44

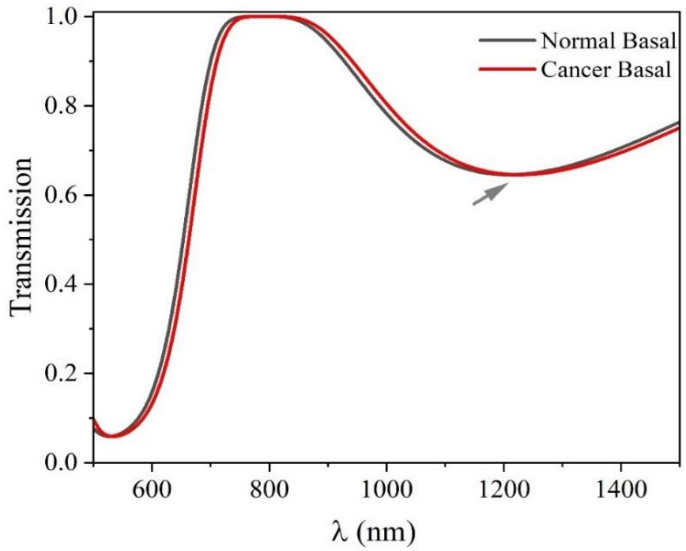


Fig. 18. Transmission spectra of the sensor structure with MoS_2 for Basal cell type with refractive indices according to Table 1.

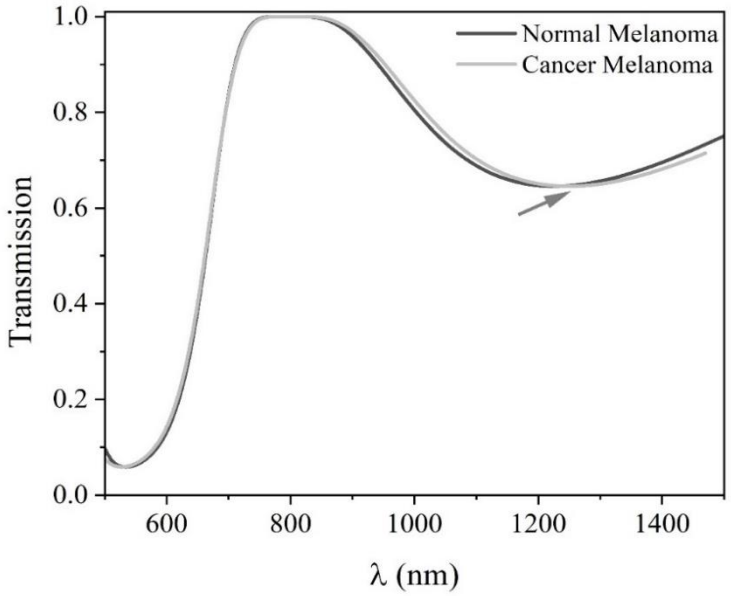


Fig. 19. Transmission spectra of the sensor structure with MoS_2 for Melanoma cell type with refractive indices according to Table 1.

We extract the resonance peak positions from the transmission spectra and determine the corresponding wavelength shifts for the healthy, basal cell, and melanoma samples. The sensitivities obtained from the linear fitting of resonance wavelength versus refractive index are presented in Figure 20. The results show a clear relationship between refractive index and resonance wavelength, with the optimized MoS_2-assisted sensor exhibiting different sensitivities for the two cancer types. A sensitivity of 880 nm/RIU is obtained for basal cell, indicating a stronger spectral response to the refractive-index difference between healthy and basal cell samples. The melanoma sample also produces a measurable resonance shift but shows a lower sensitivity. These results indicate that the optimized sensor provides a stronger optical response to basal cell samples.

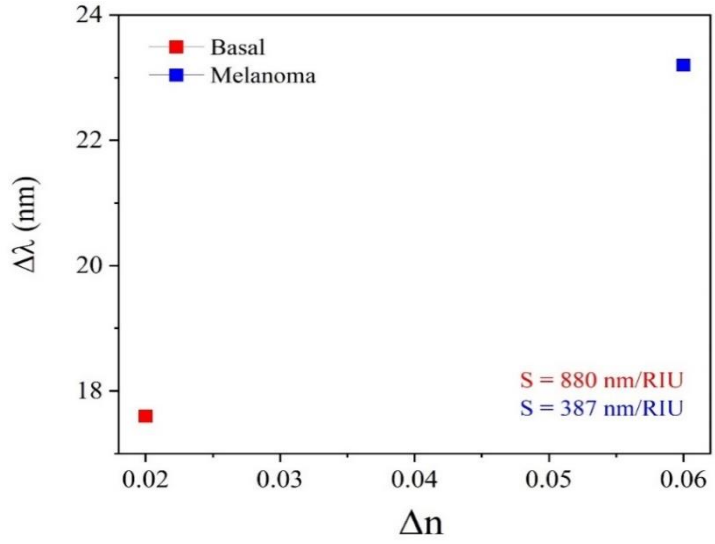


Fig. 20. Wavelength shift as a function of refractive index for Basal and Melanoma cell type the sensor based MoS_2.

To provide a clearer perspective on the sensing performance of the proposed sensor, its refractive-index sensitivity is compared with those reported for several previously published plasmonic sensors, as summarized in Table 2. The comparison includes representative MDM-based configurations with different resonator and sensing-material designs.

Table 2. Comparison of the refractive-index sensitivity of the proposed sensor with previously reported plasmonic sensors.

Ref.	Sensor Structure	Sensing Material	Sensitivity (nm/RIU)
[20]	Asymmetric MDM waveguide with a ring cavity		718
[21]	MDM waveguide with U-shaped cavity and semi-annular waveguide		825
[18]	Metal–graphene–insulator plasmonic sensor	Graphene	662.3
This work	Rectangular-tooth MDM plasmonic waveguide	MoS_2	**896**

4. Conclusion

In this work, we design and numerically analyze an MoS_2-assisted MDM plasmonic waveguide sensor with a rectangular-tooth structure for refractive-index sensing. We compare the MoS_2-based configuration with the corresponding structure without MoS_2 and with graphene under identical conditions. The sensitivity increases from 699 nm/RIU without MoS_2 to 886 nm/RIU with MoS_2, demonstrating the beneficial effect of locating MoS_2 at the metal–dielectric interface.

We further optimize the rectangular-tooth dimensions and obtain the highest sensitivity of 896 nm/RIU for a tooth size of 80 nm × 50 nm. The optimized sensor is then evaluated using the refractive indices of healthy tissue, basal cell, and melanoma samples. The results show distinct resonance shifts between the samples, with a sensitivity of 880 nm/RIU obtained for basal cell. These results confirm that the proposed MoS_2-assisted MDM sensor provides high refractive-index sensitivity and can distinguish biological samples based on their optical response.

5. Declarations Conflict of Interest

The authors declare that they have no conflict of interest.

Acknowledgments

The authors have no acknowledgments to declare.

References

[1] J. Homola, Surface plasmon resonance sensors for detection of chemical and biological species, Chemical reviews, 108 (2008) 462-493.

[2] D.K. Gramotnev, S.I. Bozhevolnyi, Plasmonics beyond the diffraction limit, Nature photonics, 4 (2010) 83-91.

[3] A. Kumar, J. Gosciniak, V.S. Volkov, S. Papaioannou, D. Kalavrouziotis, K. Vyrsokinos, J.C. Weeber, K. Hassan, L. Markey, A. Dereux, Dielectric-loaded plasmonic waveguide components: going practical, Laser & Photonics Reviews, 7 (2013) 938-951.

[4] T. Holmgaard, S.I. Bozhevolnyi, Theoretical analysis of dielectric-loaded surface plasmon-polariton waveguides, Physical Review B—Condensed Matter and Materials Physics, 75 (2007) 245405.

[5] F.J. García de Abajo, Graphene plasmonics: challenges and opportunities, ACS photonics, 1 (2014) 135-152.

[6] F. Bonaccorso, Z. Sun, T. Hasan, A.C. Ferrari, Graphene photonics and optoelectronics, Nature photonics, 4 (2010) 611-622.

[7] K.F. Mak, C. Lee, J. Hone, J. Shan, T.F. Heinz, Atomically thin MoS 2: a new direct-gap semiconductor, Physical review letters, 105 (2010) 136805.

[8] K.F. Mak, J. Shan, Photonics and optoelectronics of 2D semiconductor transition metal dichalcogenides, Nature Photonics, 10 (2016) 216-226.

[9] Z. Mao, X. Peng, Y. Zhou, Y. Liu, K. Koh, H. Chen, Review of interface modification based on 2D nanomaterials for surface plasmon resonance biosensors, Acs Photonics, 9 (2022) 3807-3823.

[10] T. Holmgaard, S.I. Bozhevolnyi, L. Markey, A. Dereux, A.V. Krasavin, P. Bolger, A.V. Zayats, Efficient excitation of dielectric-loaded surface plasmon-polariton waveguide modes at telecommunication wavelengths, Physical Review B—Condensed Matter and Materials Physics, 78 (2008) 165431.

[11] V.G. Achanta, Surface waves at metal-dielectric interfaces: Material science perspective, Reviews in Physics, 5 (2020) 100041.

[12] M. Dragoman, D. Dragoman, Plasmonics: Applications to nanoscale terahertz and optical devices, Progress in Quantum Electronics, 32 (2008) 1-41.

[13] H.-L. Liu, T. Yang, J.-H. Chen, H.-W. Chen, H. Guo, R. Saito, M.-Y. Li, L.-J. Li, Temperature-dependent optical constants of monolayer MoS 2, MoSe 2, WS 2, and WSe 2: spectroscopic ellipsometry and first-principles calculations, Scientific reports, 10 (2020) 15282.

[14] G.A. Ermolaev, Y.V. Stebunov, A.A. Vyshnevyy, D.E. Tatarkin, D.I. Yakubovsky, S.M. Novikov, D.G. Baranov, T. Shegai, A.Y. Nikitin, A.V. Arsenin, Broadband optical properties of monolayer and bulk MoS2, npj 2D Materials and Applications, 4 (2020) 21.

[15] P. Drude, Zur elektronentheorie der metalle, Annalen der physik, 306 (1900) 566-613.

[16] P.B. Johnson, R.-W. Christy, Optical constants of the noble metals, Physical review B, 6 (1972) 4370.

[17] F. Lotfi, N. Sang-Nourpour, R. Kheradmand, Graphene-based plasmonic U-shaped nanofiber biosensor: Design and analysis, Optik, 270 (2022) 169890.

[18] F. Lotfi, N. Sang-Nourpour, R. Kheradmand, Resonator-based nanoscale plasmonic sensor made of metal–graphene–insulator interfaces, Results in Physics, 64 (2024) 107922.

[19] A.C. Chaity, Highly sensitive photonic crystal fiber biosensor based on surface plasmon resonance for six distinct types of cancer detection, Plasmonics, 19 (2024) 1891-1902.

[20] X. Zhao, Z. Zhang, S. Yan, Tunable Fano resonance in asymmetric MIM waveguide structure, Sensors, 17 (2017) 1494.

[21] J. Zhu, C. Wu, Optical refractive index sensor with Fano resonance based on original MIM waveguide structure, Results in Physics, 21 (2021) 103858.